



**HAL**  
open science

## Uranium isotope geochemistry in modern coastal sediments: Insights from Toulon Bay, France

Duc Huy Dang, R. Douglas Evans, Wei Wang, Dario Omanović, Amonda El Houssainy, Véronique Lenoble, Jean-Ulrich Mullot, Stéphane Mounier, Cédric Garnier

### ► To cite this version:

Duc Huy Dang, R. Douglas Evans, Wei Wang, Dario Omanović, Amonda El Houssainy, et al.. Uranium isotope geochemistry in modern coastal sediments: Insights from Toulon Bay, France. *Chemical Geology*, 2018, 481, pp.133 - 145. 10.1016/j.chemgeo.2018.01.032 . hal-01879415

**HAL Id: hal-01879415**

**<https://hal.science/hal-01879415>**

Submitted on 29 Sep 2018

**HAL** is a multi-disciplinary open access archive for the deposit and dissemination of scientific research documents, whether they are published or not. The documents may come from teaching and research institutions in France or abroad, or from public or private research centers.

L'archive ouverte pluridisciplinaire **HAL**, est destinée au dépôt et à la diffusion de documents scientifiques de niveau recherche, publiés ou non, émanant des établissements d'enseignement et de recherche français ou étrangers, des laboratoires publics ou privés.

1                    **Uranium isotope geochemistry in modern coastal sediments:**  
2                    **insights from Toulon Bay, France**

3  
4            Duc Huy Dang<sup>1,2\*</sup>, R. Douglas Evans<sup>2,3</sup>, Wei Wang<sup>2</sup>, Dario Omanović<sup>4</sup>, Amonda El  
5            Houssainy<sup>1</sup>, Véronique Lenoble<sup>1</sup>, Jean-Ulrich Mullot<sup>5</sup>, Stéphane Mounier<sup>1</sup>, Cédric Garnier<sup>1</sup>

6  
7            <sup>1</sup> Université de Toulon, PROTEE, EA 3819, CS60584, 83041 Toulon Cedex 9, France

8            <sup>2</sup> School of the Environment and <sup>3</sup>Water Quality Centre, Trent University, 1600 West Bank  
9            Drive, Peterborough, ON, Canada K9L 0G2

10           <sup>4</sup> Center for Marine and Environmental Research, Ruđer Bošković Institute, P.O. Box 180,  
11           10002 Zagreb, Croatia

12           <sup>5</sup> LASEM-Toulon, Base Navale De Toulon, BP 61, 83800 Toulon, France

13  
14           \*Corresponding author. Tel: +1 705 748 1011 (ext. 7692).

15           *E-mail:* [huydang@trentu.ca](mailto:huydang@trentu.ca)

16

17 **ABSTRACT**

18 By assessing U geochemistry as well as U isotopic composition in marine sediments (Toulon  
19 Bay, NW Mediterranean Sea), authigenic U accumulation in sediments was found to be  
20 tightly linked to that of Mo and V with a slight difference in accumulation rate depending on  
21 sediment redox conditions and with a typical U loss in re-oxidized sediments. In sediments  
22 collected on a transect along a river plume, the authigenic accumulation of these redox-  
23 sensitive elements appears to be linked to the sediment grain size which probably drives the  
24 redox status of the sediments. The U isotopic composition in Toulon Bay sediments showed  
25 enrichment of the heavy isotope ( $\delta^{238}\text{U} = -0.12 \pm 0.12 \text{ ‰}$  relative to CRM-145 in the surface  
26 sediments). However, while U isotopic fractionation reaches half fractionation factor ( $\Delta^{238}\text{U} =$   
27  $0.6 \text{ ‰}$ ) in some sediment cores, similar to typical values observed in the literature, other cores  
28 show a full fractionation factor ( $\Delta^{238}\text{U} = 1.2 \text{ ‰}$ ). In parallel, the dissolved U profiles do not  
29 show a simple and typical depletion trend but rather a depletion in the top 10 cm followed by  
30 release below 10 cm that is probably linked to the biotic reoxidation of authigenic U(IV). The  
31 released U could be further scavenged by a competition between U-P precipitation and biotic  
32 reduction which is most likely driven by diagenetic reactions via porewater acidification and  
33 release of chelators and phosphorus.

34

35 **KEYWORDS**

36 Uranium; Coastal sediments; Diagenesis; Uranium isotope composition; Multiple regression

## 37 1. INTRODUCTION

38 The Anthropocene has been defined as the period when human (i.e., ‘anthropogenic’)  
39 activities have resulted in a significant and global impact on the Earth’s climate and  
40 ecosystems. These activities have grown exponentially over the last few decades and have led  
41 to specific geochemical signatures, distinct from natural and long-term geological processes.  
42 Understanding such processes is essential to discriminate human impacts from the natural  
43 geological signature and also to predict future variations. For example, the Earth’s  
44 oxygenation history is related to geochemical redox processes and so an understanding of  
45 these processes is indispensable for comprehending the evolution of life (Lyons et al., 2014).  
46 The exchange between the atmosphere and ocean together with seawater-sediment  
47 interactions makes marine sediments a valuable archive to evaluate past conditions. The redox  
48 sensitive elements (e.g., Mo, U, Re) have been used frequently as proxies of past redox  
49 conditions (Holmden et al., 2015; McManus et al., 2006; Siebert et al., 2003). However,  
50 further investigations on the control of geochemical processes are required in order to better  
51 use such elements as paleo-proxies. Molybdenum and U exhibit conservative behavior in  
52 oxygenated water (Chen et al., 1986; Collier, 1985) and exist in the dissolved oxyanion  
53 ( $\text{MoO}_4^{2-}$ ) or oxycation ( $\text{UO}_2^{2+}$ ) forms, but are reduced and become insoluble in anoxic  
54 conditions (Sundby et al., 2004; Yamada et al., 2006; Zheng et al., 2000). This specific  
55 character makes their authigenic formation a potential indicator of the redox boundary.  
56 Recent analytical improvements in isotope analyses have enabled the detection and  
57 measurement of small variations in U isotopic compositions. As a result, monitoring the  
58  $^{238}\text{U}/^{235}\text{U}$  ratio during U reduction and authigenic U formation in sediments has been used to  
59 interpret redox variations in the ocean (Andersen et al., 2014; Goto et al., 2014). However, U  
60 isotopic fractionation in marine conditions is still not well understood. In addition to reductive

61 reactions, other geochemical reactions such as adsorption, (co)precipitation, as well as  
62 biogenic U input could contribute to the variation in isotopic U composition (Andersen et al.,  
63 2014; Brennecka et al., 2011; Dang et al., 2016; Holmden et al., 2015; Stirling et al., 2015,  
64 2007). Even though, *ab initio* computations and experimental experiments on U biotic  
65 reduction have shown that U fractionation could reach a full fractionation factor of +1.2 ‰  
66 ( $\Delta^{238}\text{U}$ ) (Abe et al., 2008; Andersen et al., 2014; Bigeleisen, 1996; Dang et al., 2016; Fujii et  
67 al., 2006; Stylo et al., 2015), most of natural sedimentary systems record only a U-half  
68 fractionation factor ( $\Delta^{238}\text{U}$  up to +0.6‰, Andersen et al., 2016 and references therein). Recent  
69 studies suggest that a U-full fractionation factor could be observed by either a partial U  
70 removal from porewater (Andersen et al., 2014) or an early U reduction in the water column  
71 which is not transport-diffusion restricted (Andersen et al., 2017). However, this has been  
72 only observed in ancient sediments of the Black Sea (Holocene-aged sediments, Montoya-  
73 Pino et al., 2010; Weyer et al., 2008).

74 Toulon Bay (NW Mediterranean Sea) provides an interesting study site to assess the impact of  
75 human activities during the Anthropocene. The ecosystem was previously found to be highly  
76 contaminated by human activities, mainly due to World War II (Dang et al., 2015b; Tessier et  
77 al., 2011) when Toulon Bay witnessed several battles. Previous studies on Toulon Bay  
78 sediments have revealed that U, as well as Mo, Ni, Co, V and particulate organic carbon  
79 (POC) showed similar behaviors (Dang et al., 2015a). Using Principle Components Analysis  
80 (PCA) of 33 chemical parameters measured on 130 surface/deep sediment samples, Dang et  
81 al. (2015a) showed that this group of elements was negatively correlated to the group of  
82 metal/metalloid contaminants (e.g., Ag, Bi, Cd, Cu, Hg, Pb, Sn, Zn) linked to the historical  
83 pollution of Toulon Bay, suggesting either different inputs to the sediments or different  
84 diagenetic dynamics in the sediments. However, a better understanding of U geochemistry

85 and its isotopic composition in coastal sediments is required for more accurate paleo-  
86 environmental applications.

87 The purpose of this study was to study U cycling in modern coastal sediments. The study is  
88 based on a dataset including (i) U, Mo, V, POC, S, P concentrations in surface sediments (54  
89 stations within Toulon Bay) as well as data from 10 additional stations where 50-cm sediment  
90 cores were taken; (ii) U isotopic composition in 10 sediment cores and 10 surface samples and  
91 (iii) spatial and temporal variations in U and phosphate concentrations in pore waters.

92

## 93 **2. MATERIALS AND METHODS**

### 94 **2.1. Study site and sampling**

95 The samples were collected in Toulon Bay (Fig. 1, NW Mediterranean, SE French coast),  
96 which has been impacted by several anthropogenic activities including the Toulon Navy Base  
97 (different sites within the harbor), yacht clubs, marinas, small urbanized river inputs and  
98 aquaculture. Previous studies on Toulon Bay sediments revealed serious contamination of the  
99 entire ecosystem, including the sediments, seawater and biota, e.g. mussels (Dang et al.,  
100 2015a; Tessier et al., 2011). The Bay has a water residence time of 1.5 to 7.5 days (Dufresne  
101 et al., 2014), low Mediterranean tide and a low input of fresh water (from the Las and  
102 Eygoutier Rivers). The Bay also contains a seawall (Fig. 1) that divides it into two unequal  
103 parts (a small and a large bay). The sedimentation rate in the Bay was estimated from  $^{210}\text{Pb}$   
104 dating to be  $0.21 \pm 0.05 \text{ cm y}^{-1}$  (Tessier et al., 2011).

105 With the support of the French Navy (boats, materials, divers), undisturbed surface and  
106 subsurface sediments (0-5 and 5-10 cm, respectively) were collected from 54 stations situated  
107 within the whole of Toulon Bay (Fig. 1) using a sediment corer (10-cm diameter and 1-m long  
108 Plexiglas tube) that preserved the sediment water interface (SWI). In addition, sediment cores

109 (~50 cm long) were collected at ten specific stations (MIS, 3B, LAS0, LAS1, LAS2, LAS 3,  
110 12, 15, 23 and 52, Fig. 1) in order to measure parameter depth profiles both spatially (i.e.,  
111 along a pollution gradient) and temporally (i.e., seasonally).

112 Stations LAS0, LAS1, LAS2, LAS3 and 23 are situated in front of two main currently active  
113 tributaries to the Bay (the Las and Eygoutier Rivers, Fig. 1); the former Las River discharged  
114 close to station MIS before it was diverted. Stations MIS, 3B and 12 are located in active  
115 military zones with intense ship traffic and station 15 is situated in an aquaculture area (fish  
116 and mussel farming). Station 52 is located in the large bay. Samples from stations MIS, 15, 23  
117 and 52 were collected in October 2009. Sediments from station 3B and LAS0-1-2-3 were  
118 collected in February 2013 and May 2016, respectively. Additionally, 9 other sampling  
119 campaigns were carried out at station 12, starting in April 2011 and then every 2 months from  
120 May 2012 to July 2013 during which triplicate cores were obtained to determine intra-site  
121 variability (Dang et al., 2014a, 2015a). Sediments were sliced every 2 cm under inert  
122 atmosphere (N<sub>2</sub>) and centrifuged (4000 rpm, 15 min, Sigma 3-18K) within 2 h of collection.  
123 Pore waters were collected by filtration of the supernatant water (0.2- m in-line syringe  
124 filters, cellulose acetate, Sartorius) in a N<sub>2</sub>-purged glove box.

125 In the two tributaries (Las and Eygoutier), particle traps were set up by the IRSN  
126 (Radioprotection and Nuclear Safety Institute). Five particle samples were collected during a  
127 two-week period from October 2012 to May 2013, mostly during rain events (Dang et al.,  
128 2015a).

129 All solid fractions were frozen (-18°C) in HDPE bottles, freeze-dried, 2-mm sieved and then  
130 maintained at -18°C until further treatment (semi-total digestion and selective extraction).  
131 Further details regarding sediment sampling procedures and sample preparation are detailed  
132 elsewhere (Dang et al., 2015a, 2015b, 2014a, 2014b; Tessier et al., 2011).

133 **2.2. Sediment and pore water analysis**

134 A digestion was carried out on the freeze-dried sediments using aqua regia/microwave  
135 digestion (see Dang et al., 2015a; Tessier et al., 2011 for further details). Total uranium  
136 concentrations after digestion (2×54 surface/subsurface sediments, i.e., 0-5 and 5-10 cm,  
137 respectively and ~250 core slices) and in porewaters (~ 450) were determined using HR  
138 ICP/MS (Element 2, Thermo Finnigan) at the Ruđer Bošković Institute (RBI, Zagreb,  
139 Croatia). Organic carbon concentrations of these sediments and soluble reactive phosphate  
140 (SRP) in porewaters have been presented previously (Dang et al., 2014b) and are reported in  
141 the present paper to support discussions on U geochemistry.

142

143 **2.3. U stable isotope analysis**

144 For U isotope analysis, sediments were digested and recovery was verified by analysis of  
145 MESS-3 certified reference material (National Research Council of Canada). All the acid  
146 solutions were double-distilled trace metal analysis grade (BDH Aristar plus; DuoPUR,  
147 Milestone). The analytical procedures to determine U concentration and U isotope  
148 composition were detailed in a previous study (Dang et al., 2016). Briefly, U concentration  
149 was analyzed at the Water Quality Centre (WQC) at Trent University (Peterborough, Canada)  
150 using an Agilent 8800 ICP/MS (Agilent Technologies, Mississauga, Canada). Chemical  
151 separation of U from the matrix was performed using TRU resin (100-150 m, Eichrom). A  
152 double spike technique using a mixed  $^{233}\text{U}/^{236}\text{U}$  spike (IRMM-3636b) was used for internal  
153 correction of instrumental mass fractionation and potential isotope fractionation on the  
154 column (Stirling et al., 2007; Weyer et al., 2008). The U isotope measurements were  
155 performed by MC-ICP/MS (Nu Plasma II) at the WQC. Samples were introduced using a  
156 Cetac Aridus II combined with a PFA nebulizer. The U concentrations were kept at 50 ppb

157 giving a ~35 V signal on  $^{238}\text{U}$ . The contributions of  $^{235}\text{U}$  and  $^{238}\text{U}$  from the double spike  
158 solution are taken into account. The double spike correction was performed using the  
159 exponential law. Each sample was bracketed by two double-spiked standard solutions (IRMM  
160 184) and the U concentrations in samples were adjusted to  $\pm 10\%$  of that in the standards.  
161 Washout between samples was achieved using a 0.1 M HCl/0.3 M HF solution. Uranium  
162 isotope variation in the sample ( $\delta^{238}\text{U}$ ) is reported relative to that of the standard (IRMM-  
163 184), which is defined as:

$$\delta_{IRMM-184}^{238} = \left[ \frac{(^{238}\text{U}/^{235}\text{U})_{\text{sample}}}{(^{238}\text{U}/^{235}\text{U})_{IRMM-184}} - 1 \right] \times 1000$$

164 The  $^{238}\text{U}/^{235}\text{U}$  ratio in the IRMM 184 was certified to be  $137.697 \pm 0.042$  (IRMM, 2015). The  
165  $^{238}\text{U}/^{235}\text{U}$  ratios measured was  $137.697 \pm 0.019$  (2SD, n=75) using a Nu Plasma II with a  
166 long-term  $^{238}\text{U}/^{235}\text{U}$  ratio of  $137.697 \pm 0.042$  (2SD, n=235). In order to compare our data to  
167 other studies where CRM-145 was used as standard solution, a  $\Delta^{238}$  shift of -1.102 ‰ is added  
168 systematically to the  $\delta_{IRMM-184}^{238}$  to convert to  $\delta_{CRM-145}^{238}$ . Hereafter, the data on U isotopic  
169 composition are expressed relative to CRM-145.

### 170 3. RESULTS AND DISCUSSION

#### 171 3.1. Uranium distribution in sediments

172 It is important to discard different phases containing U which could be detrital U (lithogenic  
173 U) and U formed in situ (authigenic U) (Andersen et al., 2014). In Toulon Bay, we assume  
174 that the carbonate bound U is negligible as it has been assumed for the Black Sea sediments  
175 (Andersen et al., 2014; Weyer et al., 2008). Therefore, the detrital U ( $\{U_{\text{detrital}}\}$ ) is calculated  
176 based only on Al content with a detrital U/Al ratio of  $1.8 \times 10^{-5}$  (McManus et al., 2006;  
177 Tribovillard et al., 2006):

$$\{U_{detrital}\} = U/Al_{detrital} \times \{Al\}$$

178 The difference between total U and detrital U is assumed to be the authigenic U ( $\{U_{authigenic}\}$ ).  
179 Similar calculations were made for Mo and V using detrital X/Al ratios of  $1.1 \times 10^{-5}$  and  
180  $1.63 \times 10^{-3}$ ; X being Mo and V, respectively (Kyte et al., 1993; McManus et al., 2006; Morford  
181 et al., 2005; Turekian and Wedepohl, 1961).

### 182 **3.1.1. Concentrations of total Uranium**

183 The U concentration in the surface sediments of Toulon Bay averaged  $2.1 \pm 0.5 \text{ g g}^{-1}$  (n = 54,  
184 Figure 1). The lowest concentrations are observed where the tributaries of the Las and  
185 Eygoutier enter Toulon Bay (station LAS0-1-2-3, MIS and 23) and at the open part of the Bay  
186 ( $1.3 \pm 0.2 \text{ g g}^{-1}$ , n = 9). This value is close to the U concentrations measured in particles from  
187 the two tributaries ( $1.0 \pm 0.2$  and  $2.1 \pm 0.7 \text{ g g}^{-1}$  for the Las and Eygoutier, respectively).

188 The total U profiles at ten stations (Figure 2) all show an accumulation trend in the top 10-cm  
189 of the core. The uranium accumulation rate (in  $\text{g U g}^{-1} \text{ cm}^{-1}$ ) computed by integration of U  
190 concentration with depth over the first 10-cm. The values obtained (Table 1) divides the  
191 stations into two groups: the first group (stations 3B, 12, 15, 52 and MIS) has a U  
192 accumulation averaging  $0.21 \pm 0.10 \text{ g U g}^{-1} \text{ cm}^{-1}$  while at other stations (LAS0-1-2-3 and 23),  
193 only a slight U accumulation (average of  $0.04 \pm 0.05 \text{ g U g}^{-1} \text{ cm}^{-1}$ ) was observed. It should be  
194 noted that the latter five stations are situated in front of active river mouths (Las and  
195 Eygoutier, Figure 1). This increasing in U concentration could be due to either a change in  
196 delivered detrital U or in authigenic U accumulation. Moreover, the percentage of the  
197  $U_{authigenic}$  increases with depth for all ten stations (Figure S1A), starting from different initial  
198 values;  $58.8 \pm 7.7 \%$  and  $83.3 \pm 1.9 \%$  for the two respective groups (Table 1); higher authigenic  
199 U percentages are observed for the five stations in front of the river discharge. For the group  
200 including stations 3B, 12, 15, 52 and MIS, the percentage of  $U_{authigenic}$  increases with depth in

201 the subsurface sediments (Figure S1A) and a correlation between total and authigenic U  
202 accumulation slopes in the top 10 cm is observed (Fig. S1B). Below 10 cm,  $U_{\text{authigenic}}$  reaches  
203 a maximum (up to 96%). For stations LAS0-1-2-3, the  $U_{\text{authigenic}}$  fraction was stable at  
204  $87.2 \pm 3.0\%$  ( $n = 76$ ) throughout the entire core, similar to the  $U_{\text{authigenic}}$  fraction observed in  
205 the top 15-cm of station 23 ( $82.1 \pm 3.7\%$ ,  $n = 8$ ).

206 The Ti/Al ratio could indicate either a change in grain size or detrital source (Morford et al.,  
207 2005). The Ti/Al ratio over the whole Bay surface sediments is constant at  $1.4 \pm 0.4 \times 10^{-2}$   
208 ( $n=54$ ), discounting the possibility of a drastic change in detrital source in the Bay and  
209 making the Ti/Al ratio a suitable tracer of grain size. The Ti/Al ratios at ten stations are  
210 constant throughout the cores (Figure 3A, Table 1) but are particularly higher (2.5 to 3.5 fold)  
211 at station LAS0-1-2 (Table 1) compared to the average measured in the 54 surface sediment  
212 samples, indicating coarser grain sizes in LAS0, 1, and 2 (Morford et al., 2005). Below 36 cm,  
213 the Ti/Al value at station LAS2 decreased to the average seen in the Bay together with a  
214 significant accumulation of U (Figure 3B). The pollution (e.g., Hg, Ag, Bi and other metals)  
215 peak attributed to the World War II events (Dang et al., 2015a; Tessier et al., 2011), is deeper  
216 at station LAS 2 compared to the rest of the Bay (starting at -39 cm instead of -15 cm), which  
217 suggests a higher sedimentation rate at this station. The change in Ti/Al profile at station  
218 LAS2 (Figure 3B) could correspond to a change in the hydrological regime of the Las River  
219 which may have previously carried different types of particles. This could be attributed to the  
220 reinforced concrete structure that was built to definitively divert the former Las River to the  
221 current river in the 1870s (Région Provence Alpes Côte d'Azur, 2008) and/or the Dardennes  
222 dam built on the upstream of the Las River in 1912 (Laliche et al., 2015). A disruption in the  
223 nature of delivered particles would also alter the porosity of the sediments and induce a  
224 change in U accumulation (Figure 3B).

225 At the scale of the whole bay, authigenic U, Mo, V concentrations are inversely proportional  
226 to the Ti/Al ratios; this trend is more apparent at four stations in front of the Las River (Figure  
227 4). This suggests that coarser sediments are not favorable for the accumulation of these redox  
228 sensitive elements, probably because of enhanced diffusion of oxidizing species from  
229 seawater which delay diagenetic activities (refer to the SRP profiles which will be further  
230 discussed).

231 In summary, the stations situated in front of the currently active rivers (LAS0-1-2-3 and 23)  
232 are different from the other stations; U accumulation is lower at the former stations (low total  
233 concentration and higher contribution of detrital U) and begins closer to the sediment water  
234 interface (i.e., in the first cm) than at the latter stations. This could be due to differences in the  
235 input of terrestrial materials (e.g., organic matter) or a change in porosity enhancing diffusion  
236 and oxygen penetration (McManus et al., 2005).

237 In deep sediments (below 15 cm), the almost constant contribution of  $U_{\text{authigenic}}$  (Figure S1A)  
238 shows that authigenic U is preserved in sediments, except for stations 3 and MIS. In fact,  
239 previous studies have demonstrated that the sediments at stations 12, 3B and MIS have been  
240 totally (the whole MIS core) or partially mixed (from -15 to -35 cm at station 3B and some  
241 specific depths at station 12) during World War II events (Dang et al., 2015a, 2015b). These  
242 depths correspond to a loss of authigenic U (Figure S1A) probably due to oxidation during  
243 mixing events (Algeo and Maynard, 2004; Tribovillard et al., 2006). Total U profiles do not  
244 show further accumulation at depth for stations 3B, 52, MIS, LAS1 and until -35 cm for  
245 LAS2 (Figure 2). However, significant U accumulation is observed for stations 12, 15, 23 and  
246 the bottom of the LAS2 core. The redox status of the sediments and post-depositional  
247 reoxygenation would impact U geochemistry leading to the different U profiles observed in  
248 these sediment cores. This will be further discussed in the following sections.

249 The authigenic U concentrations are significantly correlated to that of Mo and V (Figure S2)  
250 because of their similar behavior, which is typical of redox-sensitive elements (Morford et al.,  
251 2009; Sundby et al., 2004; Tribovillard et al., 2006). However, they differ in their  
252 geochemistry leading to various accumulation rates depending on the redox status of the  
253 depositional environment (Algeo and Maynard, 2004; Tribovillard et al., 2006). In fact, U  
254 reduction leading to U accumulation involves soluble U(VI: mainly  $\text{UO}_2(\text{CO}_3)_3^{4-}$ ) and  
255 insoluble U(IV). This reduction could happen under denitrifying conditions (anoxia) (Algeo  
256 and Maynard, 2004; McManus et al., 2005). However, the key step leading to Mo  
257 accumulation within sediments is the sulfide activation of conservative molybdate ions to  
258 reactive thio-species (Helz et al., 1996). This step is related to sulfate-reduction and then  
259 favored in sulfidic conditions (Adelson et al., 2001). Vanadium accumulation in the sediments  
260 results from two reduction steps ( $\text{V(V)} \rightarrow \text{V(IV)} \rightarrow \text{V(III)}$ ). The first step begins in non-sulfidic  
261 anoxic environments while the latter is fostered by free sulfide (in euxinic conditions)  
262 (Tribovillard et al., 2006 and references therein).

263 Consequently, the U, Mo and V accumulate differently in the ten sediments cores when  
264 compared using linear regression (Figure S2). A multiple regression model highlights the  
265 relationship between the three elements (Table S1). Further details on the data treatment  
266 process and its validation are shown in the Supplementary Information.

267 Four groups are revealed corresponding to four relationship equations (Figures 5, S3 and  
268 Table S1). At stations 3B and MIS, a flat plane shows that authigenic U accumulation is the  
269 least important when compared to that of Mo and V concentrations (low slopes of 0.03 and  
270 0.01, for {U} vs Mo and V, respectively, Table S1, Figures 5 and S3). This confirms the  
271 hypothesis of U loss by post-depositional reoxygenation (Algeo and Maynard, 2004;  
272 Tribovillard et al., 2006) previously discussed. In the sediments at stations LAS0-1-2-3, 12,

273 52 and all surface sediments, the relationship between authigenic U and Mo was stronger than  
274 that of V (slope of 0.27 and 0.05, respectively, Table S1). In fact, authigenic V, unlike  
275 authigenic U and Mo, is only weakly enriched in these sediments when compared to the other  
276 five stations (Figure S2). The authigenic U-Mo relationships are similar at stations 23 and 15  
277 (slope of 0.45 and 0.48, respectively) while the U-V relationships are significantly different  
278 (slope of 0.06 and 0.24, respectively, Figure 4, Table S1). In addition, the accumulation zone  
279 of total S extends from the surface down to 15 cm for station 15 and to 30 cm for station 23,  
280 corresponding to a longer anoxic-to-euxinic transition at station 23 than at 15 (Figure S4). As  
281 the anoxic condition is more favorable for U and V accumulation than for Mo which is  
282 accumulated in euxinic conditions only (see discussion above), the comparison among  
283  $U_{\text{authigenic}}$ ,  $Mo_{\text{authigenic}}$ ,  $V_{\text{authigenic}}$  confirms the anoxic status at station 23 and euxinic conditions  
284 at station 15. The S content in Toulon Bay (Figure S5) shows significantly higher values  
285 along the coast (up to 1.9 %) than the open sea ( $0.38 \pm 0.06$  %,  $n = 10$ ). The S accumulation  
286 with sediment depth increases equally from the coast to the open sea (Figure S4), potentially  
287 indicating a redox gradient.

288 To summarize, the preserved sediments could be classified on an euxinic-to-anoxic gradient:  
289 15-23-52-LAS0-1-2-3. In addition, three other stations have been subjected to post-  
290 depositional reoxygenation events, from minor to total mixing (12<3B<MIS) having a direct  
291 impact on the redox status of the sediments.

### 292 **3.1.2. Uranium isotopic composition**

293 The  $\delta^{238}\text{U}$  values in the top surface sediments averaged  $-0.12 \pm 0.12$  ‰ (relative to CRM-145,  
294  $n=25$ ), close to the estimated U isotopic composition in hypoxic sediments ( $-0.24 \pm 0.08$  ‰,  
295 (Andersen et al., 2016)). When compared to the value of  $\delta^{238}\text{U}_{\text{seawater}}$  ( $-0.39 \pm 0.02$  ‰,  
296 (Noordmann et al., 2015; Romaniello et al., 2013; Tissot and Dauphas, 2015; Weyer et al.,

297 2008), U accumulation in surface sediments would lead to an enrichment of  $\Delta^{238}\text{U}_{\text{seawater-}}$   
298  $\text{sediments}$  of  $0.27\pm 0.14\text{‰}$ , similar to that observed in the oceanic crust ( $0.25\text{‰}$  (Andersen et al.,  
299 2016)) and carbonate sediments ( $0.2\text{-}0.4\text{‰}$  (Romaniello et al., 2013)).

300 In eight stations where U isotope profiles were measured, the  $\delta^{238}\text{U}$  profiles once again divide  
301 themselves into 2 groups, the first group being stations 3B, 12, 15 and 52. Station 3B showed  
302 an increasing  $\delta^{238}\text{U}$  from a value close to that of the seawater, i.e.,  $-0.37\text{‰}$  in the surface  
303 sediments to  $+0.07\text{‰}$  at the bottom of the core while stations 12, 15 and 52 displayed almost  
304 constant  $\delta^{238}\text{U}$  profiles throughout the cores ( $\delta^{238}\text{U} = -0.19\pm 0.06, -0.07\pm 0.08$  and  $-0.07\pm 0.04$   
305  $\text{‰}$ , respectively) (Figure 5). These values are comparable to the profile reported for US West  
306 Coast hypoxic margin sediment (Andersen et al., 2016). The second group, involving all  
307 stations situated close to the river mouths, has a continuously increasing  $\delta^{238}\text{U}$  signature with  
308 an average of  $-0.05\pm 0.07 \text{‰}$  in the surface sediments up to  $0.74 \text{‰}$  at 40-50 cm in the core  
309 (Figure 6).

310 Andersen et al. (2016) have gathered published literature on U isotopic composition and U  
311 accumulation in sediments and categorized them into two main groups: “hypoxic type” and  
312 “euxinic type” regarding the redox state of the water column. We have taken the Peru margin  
313 sediments reported by Andersen et al. and placed them into another plot (Figure S6) as they  
314 are organic-rich and seem to be strongly influenced by continental inputs-more so than two  
315 other types (Andersen et al., 2016; Weyer et al., 2008). Comparing our data to these three  
316 types of conditions (Figure 7A), and factoring in the oxic conditions in the water column of  
317 Toulon Bay most of sediments would be categorized as “hypoxic” thus extending the range  
318 of isotopic composition up to  $0.8\text{‰}$ .

319 Using the isotopic mass balance, the U isotopic composition in the authigenic fraction is  
320 calculated, assuming a detrital U composition of -0.3 ‰ (Andersen et al., 2014), which is  
321 close to the U isotopic composition of the Garonne and Rhone rivers (-0.32±0.04 ‰ and -  
322 0.26±0.06 ‰, respectively (Andersen et al., 2016; Tissot and Dauphas, 2015)).

$$\delta^{238}\text{U}_{\text{authigenic}} = \frac{\delta^{238}\text{U}_{\text{bulk}} - \delta^{238}\text{U}_{\text{detrital}} \times f_{\text{detrital}}}{f_{\text{authigenic}}}$$

323 With  $\delta^{238}\text{U}_{\text{bulk}}$ ,  $\delta^{238}\text{U}_{\text{detrital}}$  and  $\delta^{238}\text{U}_{\text{authigenic}}$  being the U isotopic composition of total, detrital  
324 and authigenic U and  $f_{\text{detrital}}$  and  $f_{\text{authigenic}}$  being the U distribution in these two fractions.

325 The  $\delta^{238}\text{U}_{\text{authigenic}}$  is plotted against the  $\text{U}_{\text{authigenic}}$  and compared to that in the bulk fraction  
326 (Figure 7B). Three scenarios are apparent from the three lines in Figures 7B, all starting from  
327 the U isotopic composition of seawater (-0.39‰). All the surface sediments, station MIS,  
328 LAS1, top layer of LAS2, and 52 are not highly enriched in U (up to 3 g g<sup>-1</sup> only) but U  
329 isotopes are highly fractionated. Stations 3B, 23 and the bottom layers of LAS2 display both  
330 U accumulation and isotope fractionation. Sediments from stations 12 and 15 are only slightly  
331 enriched in the heavy isotope but highly enriched in U. These two stations seem to be closer  
332 to what has been observed in the literature with the continental conditions seen in the Peru  
333 margin sediments (Andersen et al., 2016; Weyer et al., 2008). Furthermore, it should be noted  
334 that the  $\delta^{238}\text{U}$  values observed in Toulon Bay, mostly in stations MIS, LAS2 and 23 are the  
335 highest recorded in the literature in natural sediments. That said, these values are still within  
336 the theoretical range of the full U fractionation factor (+1.2‰) (Abe et al., 2008; Andersen et  
337 al., 2014; Fujii et al., 2006). Andersen et al. (2014) proposed four scenarios for how  
338 depositional environments would impact on U and U isotope accumulation in sediments. The  
339 half U fractionation factor seems to be the consensual values recorded in marine sediments  
340 worldwide (Andersen et al., 2014; Goldmann et al., 2015; Holmden et al., 2015; Montoya-

341 Pino et al., 2010; Noordmann et al., 2015; Tissot and Dauphas, 2015; Weyer et al., 2008).  
342 Most of Toulon Bay sediments fall into the “oxic penetration zone” scenario defined by  
343 Andersen et al. (2014) with half fractionation factor corresponding to a value of 0.2 ‰  
344 (Figure 7B). In addition, a possible scenario leading to such high U isotope composition (0.2-  
345 0.8‰, Andersen et al., 2014) is when U is accumulated in sediments without a full extraction  
346 of U from porewater (i.e., partial U removal). A more recent hypothesis suggests that the early  
347 U reduction in the floc layer above the sediments that is not transport-diffusion restricted  
348 would express full isotope fractionation (Andersen et al., 2017). Both these hypotheses  
349 correspond to the conditions observed at stations LAS1, LAS2, MIS and 23 (Figure 7B)  
350 where sediments are submitted to a direct delivery of terrestrial materials, probably consisting  
351 of coarse particles, which leads to a stronger diffusion compared to a well consolidated  
352 sediment pile. Also, these sediments are either post-depositionally reoxygenated (MIS) or  
353 suboxic/anoxic sediments (LAS2 and 23, see discussion above). These characteristics would  
354 lead to a full fractionation factor.

### 355 **3.2. Uranium in pore water**

356 The concentration profiles of U and SRP in pore waters at stations 3B, 12, 15, 52, LAS2-3  
357 and 23 are shown in Figures 8 and S7. The SRP results have been previously discussed (Dang  
358 et al., 2015a, 2014a, 2014b) and are shown here to support the discussion on the diagenetic  
359 behavior of U.

360 For all seven U profiles, typical U profiles in porewater (constant concentration or depletion  
361 from porewater) (Barnes and Cochran, 1993; McManus et al., 2006; Morford et al., 2005;  
362 Tribovillard et al., 2006) are observed only in the first 10 cm (Figure 8) where authigenic U  
363 formation is effective (see discussion above). Below that depth, U is strongly released in  
364 porewater. The high U concentration in the surface sediment porewater was attributed to

365 oxygen penetration (McManus et al., 2005); U release in deep sediments has not been  
366 attributed to geochemical processes but rather to either re-oxygenation of the sediment during  
367 handling or sediment oxidation by (bio)irrigation (Chaillou et al., 2002; Morford et al., 2009).  
368 However, in Toulon Bay, the absence of macrofauna and plant/algae (Bernard et al., 2001)  
369 discounts the contribution of bioirrigation and bioturbation (Dang et al., 2014b). Also, the  
370 continuously increasing sulfide profiles with depth in these cores (Dang et al., 2015a, 2014b)  
371 together with the apparent release of U in the middle of the sediment cores (Figures 8, S7)  
372 exclude the hypothesis of oxygen penetration from the bottom during coring operations.  
373 Therefore, the U release in deep anoxic/euxinic sediments is not a simple artefact but results  
374 from a specific suite of biogeochemical processes. For example, biotic oxidation of authigenic  
375 U(IV) has been shown to solubilize U (Beller, 2005; Stewart et al., 2012; Weber et al., 2011),  
376 possibly from previous U accumulation in sediments due to the reduction to U(IV) minerals  
377 (Algeo and Maynard, 2004; McManus et al., 2005). Also, studies have demonstrated that the  
378 first 10 cm of the sediments core were controlled by Mn/Fe cycling but diagenetic products  
379 ( $\text{NH}_4^+$ , SRP, DIC,  $\text{Si}(\text{OH})_4$ ) were strongly released below 15 cm, indicating a highly reactive  
380 layer (Dang et al., 2014a, 2014b). This intense diagenesis may enhance the oxidation of  
381 biogenic U(IV) either because of deviation in pH from neutral (Ginder-Vogel et al., 2010) or  
382 because of an increase in U solubility by the release of potential chelators (e.g., organic matter  
383 or carbonate) (Ginder-Vogel et al., 2010; Stewart et al., 2012). The observed increase in  
384 soluble U is supported by the significant relationship between dissolved U and sediment U  
385 (Figure 9) and highlights the redistribution between the dissolved and particulate fraction of  
386 uranium.

387 The interaction between SRP and dissolved U may also influence the redistribution of U  
388 between dissolved and particulate phases. The release of dissolved U in the presence of SRP

389 produces a precipitate and leads to a reduction in SRP. Thus an inverse relationship would be  
390 expected between SRP and dissolved uranium. In fact, at stations 15 and 23, where SRP  
391 levels are low throughout the cores dissolved U concentrations are high (up to 200-300 M  
392 U) and at stations 3 and 12, SRP concentrations are inversely proportional to U, even though  
393 the profiles of both elements vary within the core (Figures 8 and S7). This phenomenon as  
394 well seems to be affected by seasonal variations as observed at station 12 (Figure S7): the  
395 dissolved U peak at -25 cm decreases in intensity with time and with increasing SRP. At  
396 stations LAS2 and LAS3, the SRP profiles support the previous hypothesis on the diagenesis  
397 delay due to enhanced diffusion of oxidizing species from seawater. In fact, SRP (and  
398  $\text{Si(OH)}_4$ , data not shown) was strongly produced below 20 cm at station LAS2 while a release  
399 of these species was encountered from the SWI at station LAS3.

400 The pH profiles at six stations (3B, 12, 15, 23 and LAS2-3) highlight a clear difference  
401 between 3B-12-LAS2-3 and 15-23 (Figure S8). The porewaters below the sediment/water  
402 interface consistently show a lower pH value than that of the seawater (8.1-8.2). For stations  
403 3B and 12, this value remains stable for the first 20 cm then markedly decreases down to 6.5  
404 below 20 cm. Alternately, the porewater pH at stations 15 and 23 is constant at a value of  
405  $7.7 \pm 0.1$  (n=48) throughout the whole core. A similar trend was observed for the redistribution  
406 between protein-like and humic like fluorophores at these stations (Dang et al., 2014a,  
407 2014b); dominance of protein-like organic matter in the top 20 cm is followed by a switch to  
408 humic-like organic matter below 20 cm at station 12, while at station 15 (sediment core  
409 collected on November 2009) a dominance of protein-like organic matter occurs throughout  
410 the whole core. These observations confirm strong diagenetic reactions below 20 cm at  
411 stations 3B and 12, while a constant and weaker reactivity was observed at stations 15 and 23  
412 (Dang et al., 2014a, b).

413 The U-P precipitation system in a seawater matrix at different pH values was modeled with  
414 PHREEQC (version 2.18.3,40) similar to an approach previously described (Dang et al.,  
415 2016). Briefly, the chemical speciation and the mineral saturation index in mixtures consisting  
416 of U and P (in the concentration range of our samples: 1 to 500 nM and 1  $\mu$ M to 100 M,  
417 respectively) in the seawater matrix was calculated (Figure S9) for a range of pH values (6-8)  
418 that are relevant when considering the observed variations in the porewaters. Negative values  
419 suggest that the formation of the concerned mineral is not thermodynamically favored while  
420 increasing values to zero show higher potential for mineral precipitation. At the concentration  
421 range found in Toulon Bay sediments, the formation of Na-autunite is more favored with a  
422 decreasing pH (Figure S9); concretely speaking, U-P precipitation is more probable at stations  
423 3B and 12 than at stations 15 and 23.

424 In summary, the situations in which high U release is observed (stations 15 and 23)  
425 correspond to a low-to-intermediate diagenetic reactivity (i.e., lower pH, less SRP  
426 production). Therefore, U removal relies only on U reduction, the intensity of which may be  
427 different depending on the redox status of the sediments and on bacterial activities. Previous  
428 work has demonstrated that the dissolved organic matter at station 15 is dominated by protein-  
429 like fluorophores, potentially related to the location of this station near an aquaculture area  
430 (Dang et al., 2014b). In the reverse case, when diagenetic activities are more intense,  
431 porewater tends to be SRP-richer and decreases in pH, conditions for which the precipitation  
432 of U-P mineral competes with U biotic reduction. Moreover, U-P precipitation does not  
433 induce U isotopic fractionation while U biotic reduction does with a full fractionation factor  
434 of 1.2 ‰ (Andersen et al., 2016; Dang et al., 2016; Stylo et al., 2015). This competition  
435 between biotic reduction of U and biomineralization of U-P minerals has already been  
436 observed in a previous study (Salome et al., 2013).

437

#### 438 **4. CONCLUSIONS**

439 The dataset obtained on U isotope geochemistry permits a better understanding of U cycling  
440 in modern coastal sediments. The impact of terrestrial particle size has been demonstrated to  
441 be directly driving the accumulation of U, Mo and V via the redox status of the sediments.  
442 Also, the impact of human activities on sediment integrity induces variations in elemental  
443 geochemistry that differ from other systems where U isotopic compositions have been  
444 recorded (Andersen et al., 2016 and references therein). This study has reported a full U  
445 fractionation factor in modern sediments which has been previously reported only in  
446 Holocene-aged sediments of the Black Sea. These data support that enhanced diffusion in  
447 coarser sediments could supply a larger U amount than in a compact sediment pile and that  
448 could lead to a more effective U isotope fractionation. In addition, this study reports an  
449 anaerobic oxidation of authigenic U(IV) which leads to a strong release of dissolved U in  
450 deep porewater. The trapping effect of SRP on the released U is attributed to strong diagenetic  
451 activities leading to increasing insolubility of U-P minerals. Also, as U precipitation in  
452 phosphate mineral does not induce isotopic fractionation, we suggest that the contribution of  
453 SRP may alter the full U fractionation factor and SRP release is driven by the redox status of  
454 the sediments (indirectly linked to diagenesis and sediment characteristics). However, further  
455 studies are required to further test these hypotheses as the atypical dissolved U profiles and  
456 high U isotopic composition have not been observed previously in the literature.

457

#### 458 **ACKNOWLEDGEMENTS:**

459 This study was part of the MerMex-WP3-C3A/MISTRALS research program (part of the  
460 international IMBER, LOICZ and SOLAS projects), and funded through the CARTOCHIM,

461 CARTOC, PREVENT and METFLUX research programs (funded by "Toulon-Provence-  
462 Méditerranée (TPM)", the "Région PACA", and "l'Agence de l'Eau Rhône-Méditerranée et  
463 Corse"). DHD's Ph.D. and postdoctoral fellowship were respectively supported by the French  
464 Ministry of National Education, Higher Education and Research and a Canadian NSERC  
465 (Natural Sciences and Engineering Research Council) Collaborative Research and  
466 Development Grant to RDE, which also funded the analyses carried out at the Trent WQC.  
467 The authors wish to thank the French Navy for diving and sampling assistance, Dr. Bastian  
468 Georg for assistance with isotope measurements and Dr. Hayla Evans for English correction  
469 and manuscript revision.

470

## 471 REFERENCES

- 472 Abe, M., Suzuki, T., Fujii, Y., Hada, M., Hirao, K., 2008. Ligand effect on uranium isotope  
473 fractionations caused by nuclear volume effects: An ab initio relativistic molecular  
474 orbital study. *J. Chem. Phys.* 129, 164309. doi:10.1063/1.3463797
- 475 Adelson, J.M., Helz, G.R., Miller, C. V., 2001. Reconstructing the rise of recent coastal  
476 anoxia; molybdenum in Chesapeake Bay sediments. *Geochim. Cosmochim. Acta* 65,  
477 237–252. doi:10.1016/S0016-7037(00)00539-1
- 478 Algeo, T.J., Maynard, J.B., 2004. Trace-element behavior and redox facies in core shales of  
479 Upper Pennsylvanian Kansas-type cyclothems. *Chem. Geol.* 206, 289–318.  
480 doi:10.1016/j.chemgeo.2003.12.009
- 481 Andersen, M.B., Romaniello, S., Vance, D., Little, S.H., Herdman, R., Lyons, T.W., 2014. A  
482 modern framework for the interpretation of  $^{238}\text{U}/^{235}\text{U}$  in studies of ancient ocean  
483 redox. *Earth Planet. Sci. Lett.* 400, 184–194. doi:10.1016/j.epsl.2014.05.051
- 484 Andersen, M.B., Stirling, C.H., Weyer, S., 2017. Uranium Isotope Fractionation, in: Teng, F.-  
485 Z., Watkins, J., Dauphas, N. (Eds.), *Reviews in Mineralogy & Geochemistry*. pp. 799–  
486 850.
- 487 Andersen, M.B., Vance, D., Morford, J.L., Bura-Nakić, E., Breitenbach, S.F.M., Och, L.,

- 488 2016. Closing in on the marine  $^{238}\text{U}/^{235}\text{U}$  budget. *Chem. Geol.* 420, 11–22.  
489 doi:10.1016/j.chemgeo.2015.10.041
- 490 Barnes, C.E., Cochran, J.K., 1993. Uranium geochemistry in estuarine sediments: Controls on  
491 removal and release processes. *Geochim. Cosmochim. Acta* 57, 555–569.  
492 doi:10.1016/0016-7037(93)90367-6
- 493 Beller, H.R., 2005. Anaerobic, nitrate-dependent oxidation of U (IV) oxide minerals by the  
494 chemolithoautotrophic Bacterium *Thiobacillus denitrificans*. *Appl. Environ. Microbiol.*  
495 2170–2174. doi:10.1128/AEM.71.4.2170
- 496 Bernard, G., Denis, J., Deneux, F., Belsher, T., Sauzade, D., Boudouresque, C.F., Charbonnel,  
497 E., Emery, E., Herve, G., Bonhomme, P., 2001. Etude et cartographie des biocénoses de  
498 la rade de Toulon, in: Contrat D'étude Pour Le Syndicat Intercommunal de l'Aire  
499 Toulonnaise, Ifremer et GISPosidonie. Ifremer Publ, La Seyne, p. 150.
- 500 Bigeleisen, J., 1996. Nuclear size and shape effects in chemical reactions. Isotope chemistry  
501 of the heavy elements. *J. Am. Chem. Soc.* 118, 3676–3680. doi:10.1021/ja954076k
- 502 Brennecka, G., Wasylenki, L.E., Weyer, S., Anbar, a D., 2011. Uranium isotope fractionation  
503 during adsorption to manganese oxides. *Environ. Scienc Technol.* 1370–1375.
- 504 Chaillou, G., Anschutz, P., Lavaux, G., Schäfer, J., Blanc, G., 2002. The distribution of Mo,  
505 U, and Cd in relation to major redox species in muddy sediments of the Bay of Biscay.  
506 *Mar. Chem.* 80, 41–59. doi:10.1016/S0304-4203(02)00097-X
- 507 Chen, J.H., Lawrence Edwards, R., Wasserburg, G.J., 1986.  $^{238}\text{U}$ ,  $^{234}\text{U}$  and  $^{232}\text{Th}$  in  
508 seawater. *Earth Planet. Sci. Lett.* 80, 241–251. doi:10.1016/0012-821X(86)90108-1
- 509 Collier, R.W., 1985. Molybdenum in the Northeast Pacific Ocean. *Limnol. Oceanogr.* 30,  
510 1351–1354. doi:10.4319/lo.1985.30.6.1351
- 511 Dang, D.H., Breda, N., Wang, W., Georg, R.B., Evans, D., 2016. Uranium isotope  
512 fractionation during adsorption, (co)precipitation and biotic reduction. *Environ. Sci.*  
513 *Technol.* 50, 12695–12704.
- 514 Dang, D.H., Lenoble, V., Durrieu, G., Mullot, J.-U., Mounier, S., Garnier, C., 2014a.  
515 Sedimentary dynamics of coastal organic matter: An assessment of the porewater  
516 size/reactivity model by spectroscopic techniques. *Estuar. Coast. Shelf Sci.* 151, 100–

517 111. doi:10.1016/j.ecss.2014.10.002

518 Dang, D.H., Lenoble, V., Durrieu, G., Omanović, D., Mullot, J.-U., Mounier, S., Garnier, C.,  
519 2015a. Seasonal variations of coastal sedimentary trace metals cycling: Insight on the  
520 effect of manganese and iron (oxy)hydroxides, sulphide and organic matter. *Mar. Pollut.*  
521 *Bull.* 92, 113–124. doi:10.1016/j.marpolbul.2014.12.048

522 Dang, D.H., Schaefer, J., Brach-Papa, C., Lenoble, V., Durrieu, G., Dutruch, L., Chiffoleau,  
523 J.-F., Gonzalez, J.-L., Blanc, G., Mullot, J.U., Mounier, S., Garnier, C., 2015b.  
524 Evidencing the impact of coastal contaminated sediments on mussels through Pb stable  
525 isotopes composition. *Environ. Sci. Technol.* 49, 11438–11448.  
526 doi:10.1021/acs.est.5b01893

527 Dang, D.H., Tessier, E., Lenoble, V., Durrieu, G., Omanović, D., Mullot, J.-U., Pfeifer, H.-R.,  
528 Mounier, S., Garnier, C., 2014b. Key parameters controlling arsenic dynamics in coastal  
529 sediments: an analytical and modeling approach. *Mar. Chem.* 161, 34–46.

530 Dufresne, C., Duffa, C., Rey, V., 2014. Wind-forced circulation model and water exchanges  
531 through the channel in the Bay of Toulon. *Ocean Dyn.* 64, 209–224.  
532 doi:10.1007/s10236-013-0676-3

533 Fujii, Y., Higuchi, N., Haruno, Y., Nomura, M., Suzuki, T., 2006. Temperature dependence of  
534 isotope effects in uranium chemical exchange reactions. *J. Nucl. Sci. Technol.* 43, 400–  
535 406. doi:10.1080/18811248.2006.9711111

536 Ginder-Vogel, M., Stewart, B., Fendorf, S., 2010. Kinetic and mechanistic constraints on the  
537 oxidation of biogenic uraninite by ferrihydrite. *Environ. Sci. Technol.* 44, 163–169.  
538 doi:10.1021/es902452u

539 Goldmann, A., Brenneka, G., Noordmann, J., Weyer, S., Wadhwa, M., 2015. The uranium  
540 isotopic composition of the Earth and the Solar System. *Geochim. Cosmochim. Acta*  
541 148, 145–158. doi:10.1016/j.gca.2014.09.008

542 Goto, K.T., Anbar, A.D., Gordon, G.W., Romaniello, S.J., Shimoda, G., Takaya, Y.,  
543 Tokumaru, A., Nozaki, T., Suzuki, K., Machida, S., Hanyu, T., Usui, A., 2014. Uranium  
544 isotope systematics of ferromanganese crusts in the Pacific Ocean: Implications for the  
545 marine  $^{238}\text{U}/^{235}\text{U}$  isotope system. *Geochim. Cosmochim. Acta* 146, 43–58.

546 doi:10.1016/j.gca.2014.10.003

547 Helz, G.R., Miller, C. V., Charnock, J.M., Mosselmans, J.F.W., Patrick, R. a D., Garner,  
548 C.D., Vaughan, D.J., 1996. Mechanism of molybdenum removal from the sea and its  
549 concentration in black shales: EXAFS evidence. *Geochim. Cosmochim. Acta* 60, 3631–  
550 3642. doi:10.1016/0016-7037(96)00195-0

551 Holmden, C., Amini, M., Francois, R., 2015. Uranium isotope fractionation in Saanich Inlet:  
552 A modern analog study of a paleoredox tracer. *Geochim. Cosmochim. Acta* 153, 202–  
553 215. doi:10.1016/j.gca.2014.11.012

554 IRMM, 2015. Nuclear certified reference materials, Institute for Reference Materials and  
555 Measurements (IRMM). Geel, Belgium.

556 Kyte, F.T., Leinen, M., Ross Heath, G., Zhou, L., 1993. Cenozoic sedimentation history of the  
557 central North Pacific: Inferences from the elemental geochemistry of core LL44-GPC3.  
558 *Geochim. Cosmochim. Acta* 57, 1719–1740. doi:10.1016/0016-7037(93)90109-A

559 Laliche, K., Venier, R., Degoutte, G., Meriaux, P., Patouillet, B., Bailleul, J., Laliche, K.,  
560 Venier, R., Degoutte, G., Meriaux, P., Patouillet, B., 2015. Dardennes dam: foundation  
561 investigations and diagnosis before reinforcement studies, in: Colloque CFBR ”  
562 Fondations Des Barrages : Caracterisation, Traitements, Surveillance, Rehabilitation ”.

563 Lyons, T.W., Reinhard, C.T., Planavsky, N.J., 2014. The rise of oxygen in Earth’s early ocean  
564 and atmosphere. *Nature* 506, 307–15. doi:10.1038/nature13068

565 McManus, J., Berelson, W.M., Klinkhammer, G.P., Hammond, D.E., Holm, C., 2005.  
566 Authigenic uranium: Relationship to oxygen penetration depth and organic carbon rain.  
567 *Geochim. Cosmochim. Acta* 69, 95–108. doi:10.1016/j.gca.2004.06.023

568 McManus, J., Berelson, W.M., Severmann, S., Poulson, R.L., Hammond, D.E., Klinkhammer,  
569 G.P., Holm, C., 2006. Molybdenum and uranium geochemistry in continental margin  
570 sediments: Paleoproxy potential. *Geochim. Cosmochim. Acta* 70, 4643–4662.  
571 doi:10.1016/j.gca.2006.06.1564

572 Montoya-Pino, C., Weyer, S., Anbar, A.D., Pross, J., Oschmann, W., van de Schootbrugge,  
573 B., Arz, H.W., 2010. Global enhancement of ocean anoxia during oceanic anoxic event  
574 2: A quantitative approach using U isotopes. *Geology* 38, 315–318.

575 doi:10.1130/G30652.1

576 Morford, J.L., Emerson, S.R., Breckel, E.J., Kim, S.H., 2005. Diagenesis of oxyanions (V, U,  
577 Re, and Mo) in pore waters and sediments from a continental margin. *Geochim.*  
578 *Cosmochim. Acta* 69, 5021–5032. doi:10.1016/j.gca.2005.05.015

579 Morford, J.L., Martin, W.R., François, R., Carney, C.M., 2009. A model for uranium,  
580 rhenium, and molybdenum diagenesis in marine sediments based on results from coastal  
581 locations. *Geochim. Cosmochim. Acta* 73, 2938–2960. doi:10.1016/j.gca.2009.02.029

582 Noordmann, J., Weyer, S., Montoya-Pino, C., Dellwig, O., Neubert, N., Eckert, S., Paetzel,  
583 M., Böttcher, M.E., 2015. Uranium and molybdenum isotope systematics in modern  
584 euxinic basins: Case studies from the central Baltic Sea and the Kyllaren fjord (Norway).  
585 *Chem. Geol.* 396, 182–195. doi:10.1016/j.chemgeo.2014.12.012

586 Région Provence Alpes Côte d’Azur, 2008. Le Las : Une Rivière dans la Ville. Val d’As,  
587 Toulon.

588 Romaniello, S.J., Herrmann, A.D., Anbar, A.D., 2013. Uranium concentrations and  
589  $^{238}\text{U}/^{235}\text{U}$  isotope ratios in modern carbonates from the Bahamas: Assessing a novel  
590 paleoredox proxy. *Chem. Geol.* 362, 305–316. doi:10.1016/j.chemgeo.2013.10.002

591 Salome, K.R., Green, S.J., Beazley, M.J., Webb, S.M., Kostka, J.E., Taillefert, M., 2013. The  
592 role of anaerobic respiration in the immobilization of uranium through biomineralization  
593 of phosphate minerals. *Geochim. Cosmochim. Acta* 106, 344–363.  
594 doi:10.1016/j.gca.2012.12.037

595 Siebert, C., Nägler, T.F., von Blanckenburg, F., Kramers, J.D., 2003. Molybdenum isotope  
596 records as a potential new proxy for paleoceanography. *Earth Planet. Sci. Lett.* 211, 159–  
597 171. doi:10.1016/S0012-821X(03)00189-4

598 Stewart, B.D., Girardot, C., Spycher, N., Sani, R.K., Peyton, B.M., 2012. Influence of  
599 chelating agents on biogenic uraninite reoxidation by Fe(III) (hydr)oxides. *Environ. Sci.*  
600 *Technol.* 47, 364–371. doi:10.1021/es303022p

601 Stirling, C.H., Andersen, M.B., Potter, E.K., Halliday, A.N., 2007. Low-temperature isotopic  
602 fractionation of uranium. *Earth Planet. Sci. Lett.* 264, 208–225.  
603 doi:10.1016/j.epsl.2007.09.019

- 604 Stirling, C.H., Andersen, M.B., Warthmann, R., Halliday, A.N., 2015. Isotope fractionation of  
605  $^{238}\text{U}$  and  $^{235}\text{U}$  during biologically-mediated uranium reduction. *Geochim. Cosmochim.*  
606 *Acta* 163, 200–218. doi:10.1016/j.gca.2015.03.017
- 607 Stylo, M., Neubert, N., Wang, Y., Monga, N., Romaniello, S.J., Weyer, S., Bernier-Latmani,  
608 R., 2015. Uranium isotopes fingerprint biotic reduction. *Proc. Natl. Acad. Sci. U. S. A.*  
609 112, 5619–24. doi:10.1073/pnas.1421841112
- 610 Sundby, B., Martinez, P., Gobeil, C., 2004. Comparative geochemistry of cadmium, rhenium,  
611 uranium, and molybdenum in continental margin sediments. *Geochim. Cosmochim. Acta*  
612 68, 2485–2493. doi:10.1016/j.gca.2003.08.011
- 613 Tessier, E., Garnier, C., Mullet, J.-U., Lenoble, V., Arnaud, M., Raynaud, M., Mounier, S.,  
614 2011. Study of the spatial and historical distribution of sediment inorganic contamination  
615 in the Toulon bay (France). *Mar. Pollut. Bull.* 62, 2075–2086.  
616 doi:10.1016/j.marpolbul.2011.07.022
- 617 Tissot, F.L.H., Dauphas, N., 2015. Uranium isotopic compositions of the crust and ocean:  
618 Age corrections, U budget and global extent of modern anoxia. *Geochim. Cosmochim.*  
619 *Acta* 167, 113–143. doi:10.1016/j.gca.2015.06.034
- 620 Tribouvillard, N., Algeo, T.J., Lyons, T., Riboulleau, A., 2006. Trace metals as paleoredox and  
621 paleoproductivity proxies: An update. *Chem. Geol.* 232, 12–32.  
622 doi:10.1016/j.chemgeo.2006.02.012
- 623 Turekian, K.K., Wedepohl, K.H., 1961. Geological Society of America Bulletin Distribution  
624 of the Elements in Some Major Units of the Earth's Crust. *Geol. Soc. Am. Bull.* 72,  
625 175–192. doi:10.1130/0016-7606(1961)72
- 626 Weber, K.A., Cameron Thrash, J., Ian Van Trump, J., Achenbach, L.A., Coates, J.D., 2011.  
627 Environmental and taxonomic bacterial diversity of anaerobic uranium(IV) bio-  
628 oxidation. *Appl. Environ. Microbiol.* 77, 4693–4696. doi:10.1128/AEM.02539-10
- 629 Weyer, S., Anbar, a. D., Gerdes, a., Gordon, G.W., Algeo, T.J., Boyle, E. a., 2008. Natural  
630 fractionation of  $^{238}\text{U}/^{235}\text{U}$ . *Geochim. Cosmochim. Acta* 72, 345–359.  
631 doi:10.1016/j.gca.2007.11.012
- 632 Yamada, M., Wang, Z.-L., Kato, Y., 2006. Precipitation of authigenic uranium in suboxic

633 continental margin sediments from the Okinawa Trough. *Estuar. Coast. Shelf Sci.* 66,  
634 570–579. doi:10.1016/j.ecss.2005.11.002

635 Zheng, Y., Anderson, R.F., Van Geen, A., Kuwabara, J., 2000. Authigenic molybdenum  
636 formation in marine sediments: A link to pore water sulfide in the Santa Barbara Basin.  
637 *Geochim. Cosmochim. Acta* 64, 4165–4178. doi:10.1016/S0016-7037(00)00495-6

638

## TABLES

**Table 1:** U accumulation rate (integration of U concentration with depth), percentage of authigenic U in the top surface sediments and Ti/Al ratios at ten sediment cores in Toulon Bay.

## FIGURES

**Figure 1:** Map of the study site with the main anthropogenic activities and locations of the 54 surface (0–5 cm) sediment samples (crosses) and 10 interface sediment cores (black circles). Uranium concentrations in surface sediments of the 54 stations are also shown. White labels show surface sediments where U isotope composition was analyzed.

**Figure 2:** Uranium profiles in sediment cores at ten stations.

**Figure 3:** (A) Vertical profile of Ti/Al at ten stations, the vertical line and the grey zone indicates the average value and the range of Ti/Al for the 54 stations in the whole bay. (B) A comparison of the vertical Ti/Al ratios and total U concentrations at station LAS2.

**Figure 4:** Authigenic U, Mo and V concentrations vs. Ti/Al ratios in sediments at stations LAS 0-1-2-3 (green circles) and MIS, 3B, 12, 15, 23, 52 and surface sediments (blue circles).

**Figure 5:** A multiple regression model of authigenic U as a function of authigenic Mo and V. Four configurations are displayed and individual plots are shown in Figure S3. The  $r^2$  values correspond to the relationship between observed vs. calculated authigenic U.

**Figure 6:** Vertical profiles of U isotopic composition at eight stations, the vertical line and blue zone show the value and range of  $\delta^{238}\text{U}$  in seawater. The grey circles display the U isotopic profile in sediments at the US West Coast (Andersen et al., 2016).

**Figure 7:** (A) Total U versus U isotopic composition in Toulon Bay and also three types of sediments gathered from the literature (11 individual datasets are shown in Figure S6). (B) Uranium concentration versus U isotopic composition in the authigenic fraction (semi-filled symbols) and the bulk sediments (grey symbols) in Toulon Bay. The vertical line and blue zone display the U isotopic composition of seawater, the vertical bold line shows the full U fractionation factor from seawater ( $\Delta^{238}\text{U} = 1.2 \text{ ‰}$ ). The two configurations: Oxidic penetration zone and Partial U porewater removal correspond to the half-U fractionation and full-U fractionation factors defined by Andersen et al. (2014)

**Figure 8:** Dissolved U and SRP profiles at seven stations. The grey zone at station 12 shows intra-site variation on triplicate cores while the dashed line indicates the range of seasonal variation for 10 cores. The grey zone in the U plots for stations 3B, 12 and 52 corresponds to that in stations 15, LAS2-3 and 23 to better highlight the difference in axis scaling.

**Figure 9:** Relationship between dissolved and total U at seven stations.

Figure 1

[Click here to download high resolution image](#)

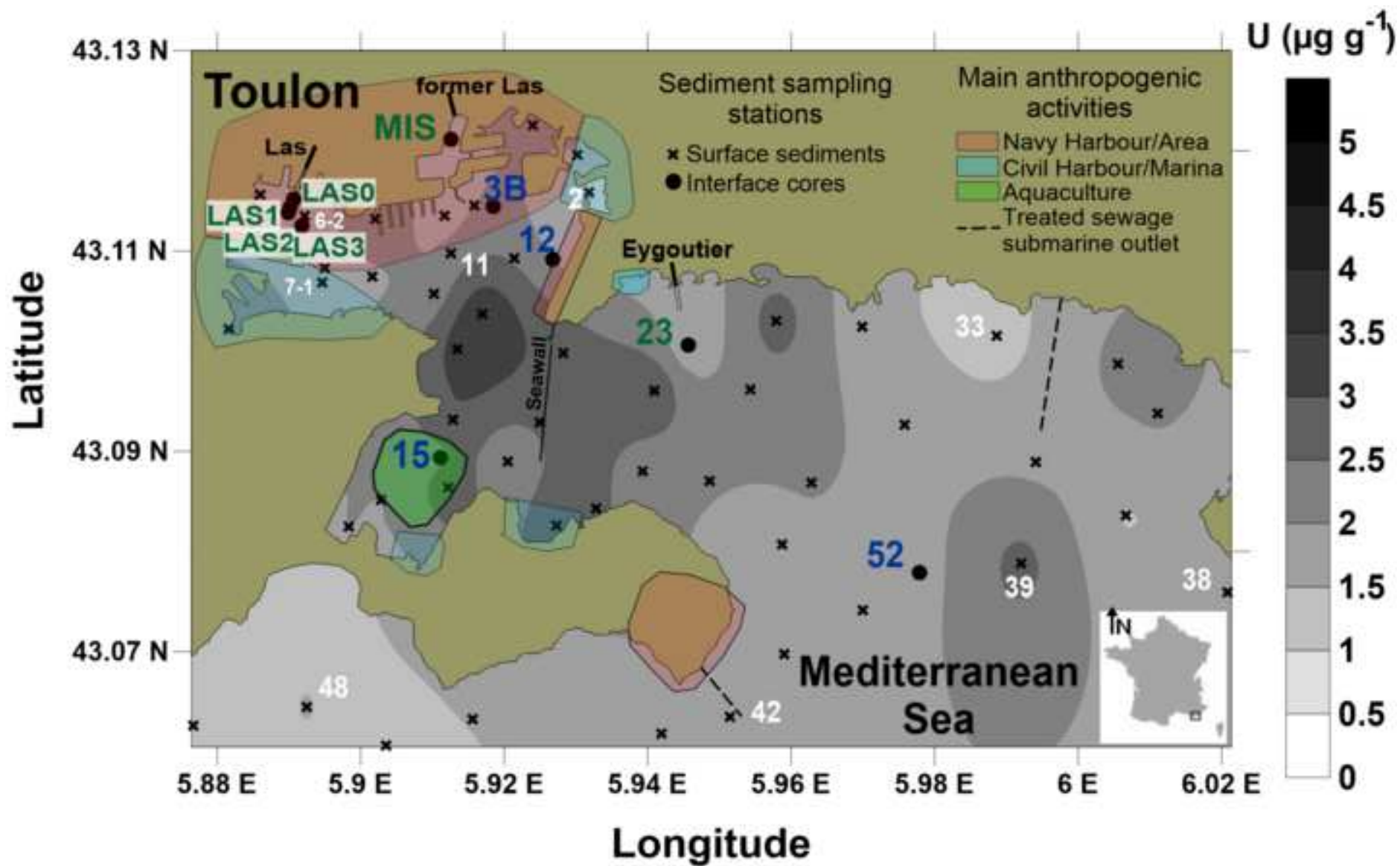




Figure 3

[Click here to download high resolution image](#)

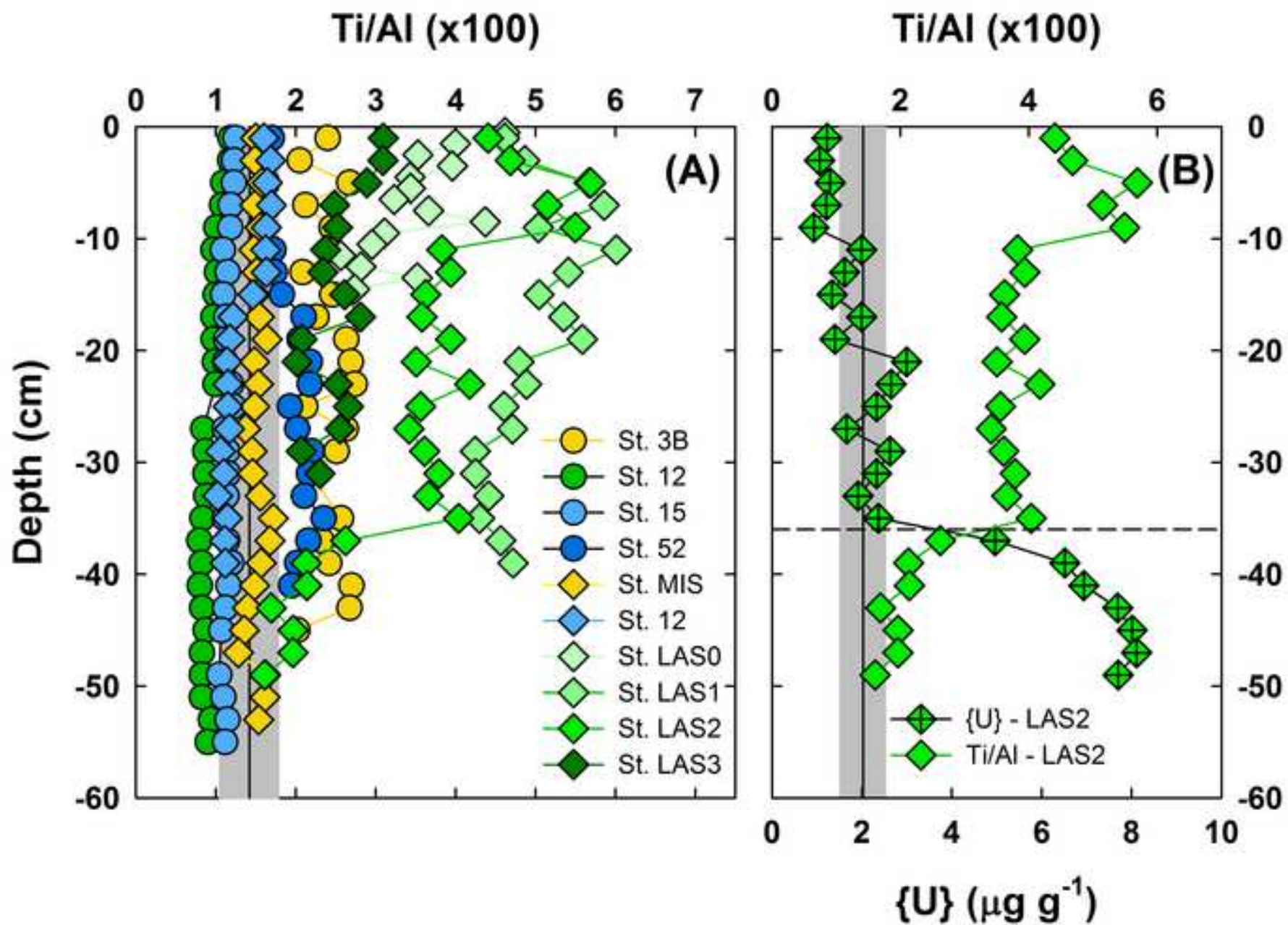


Figure 4  
[Click here to download high resolution image](#)

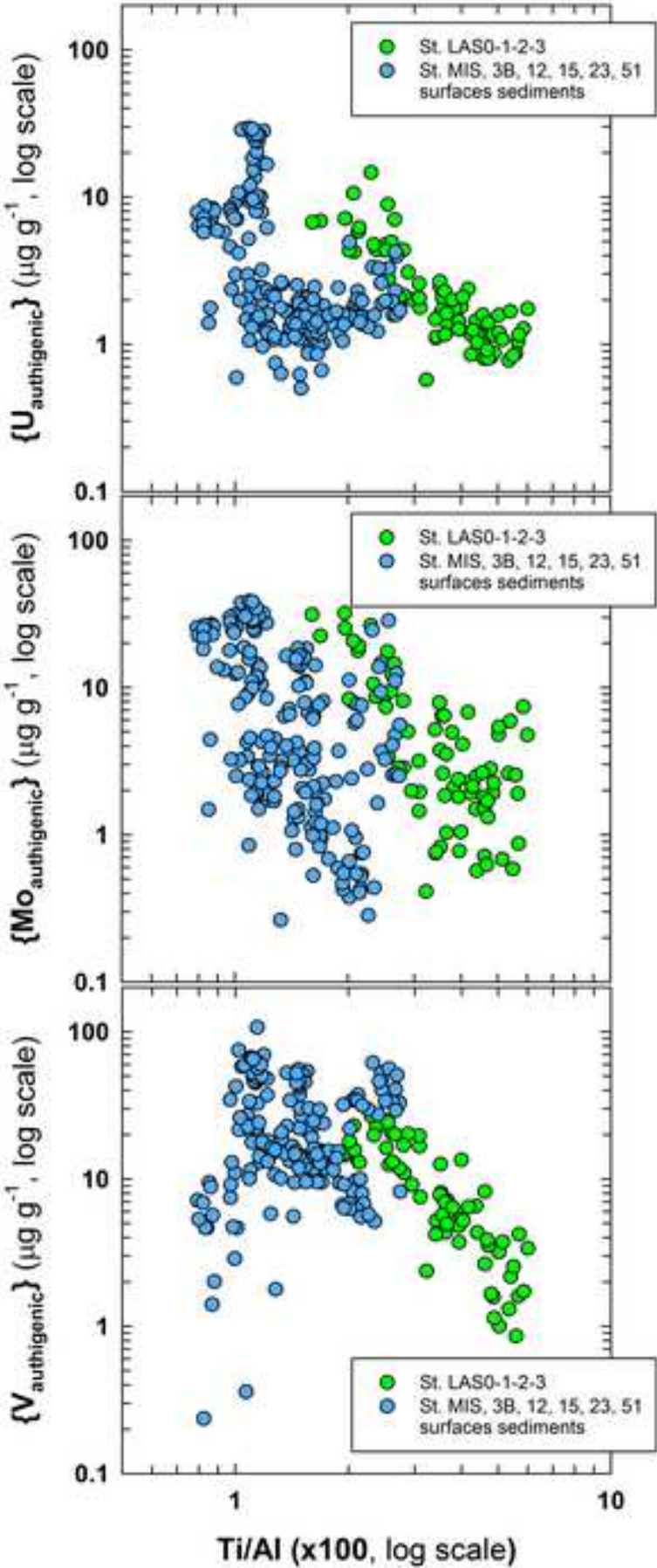


Figure 5  
[Click here to download high resolution image](#)

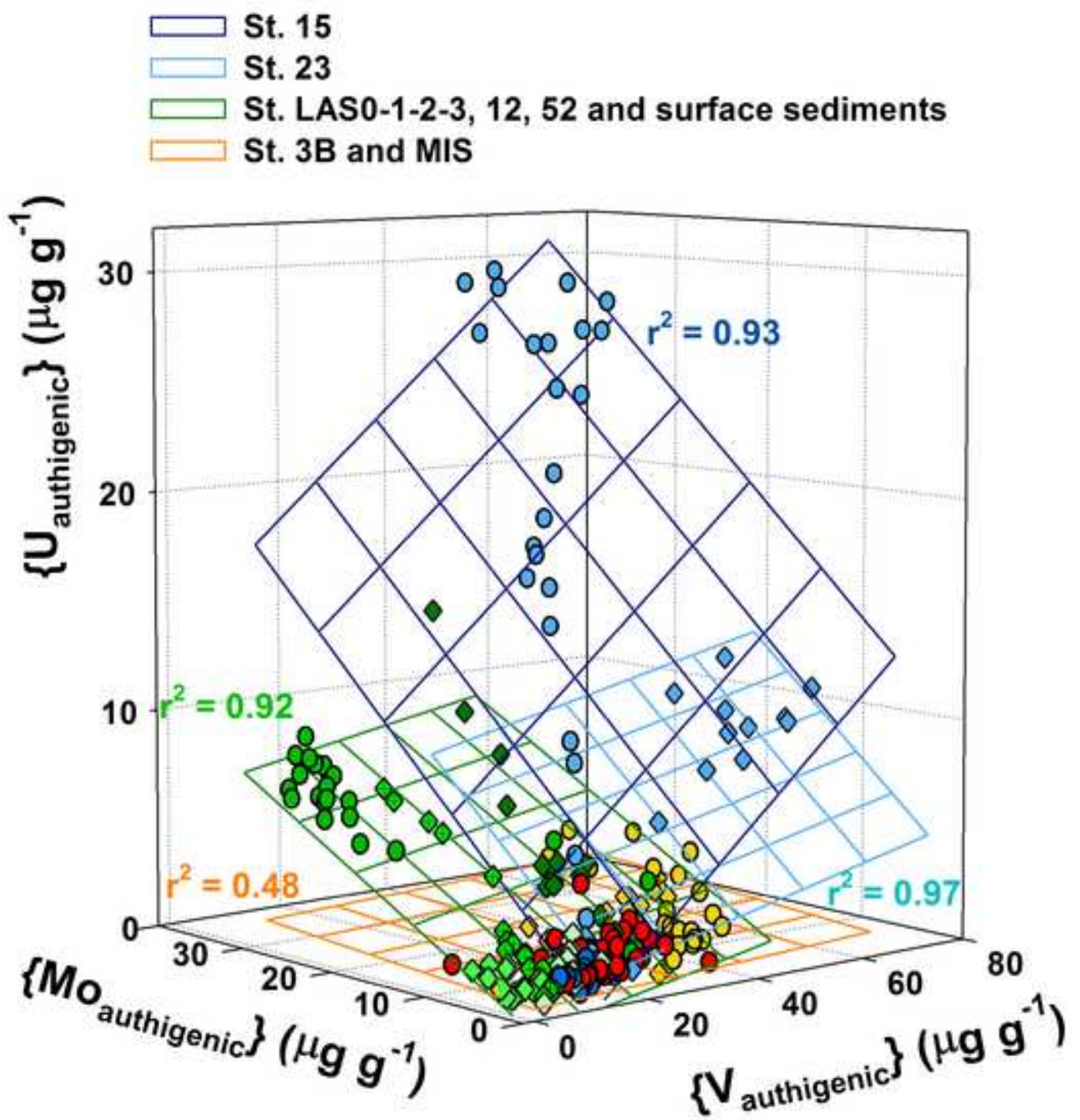


Figure 6

[Click here to download high resolution image](#)

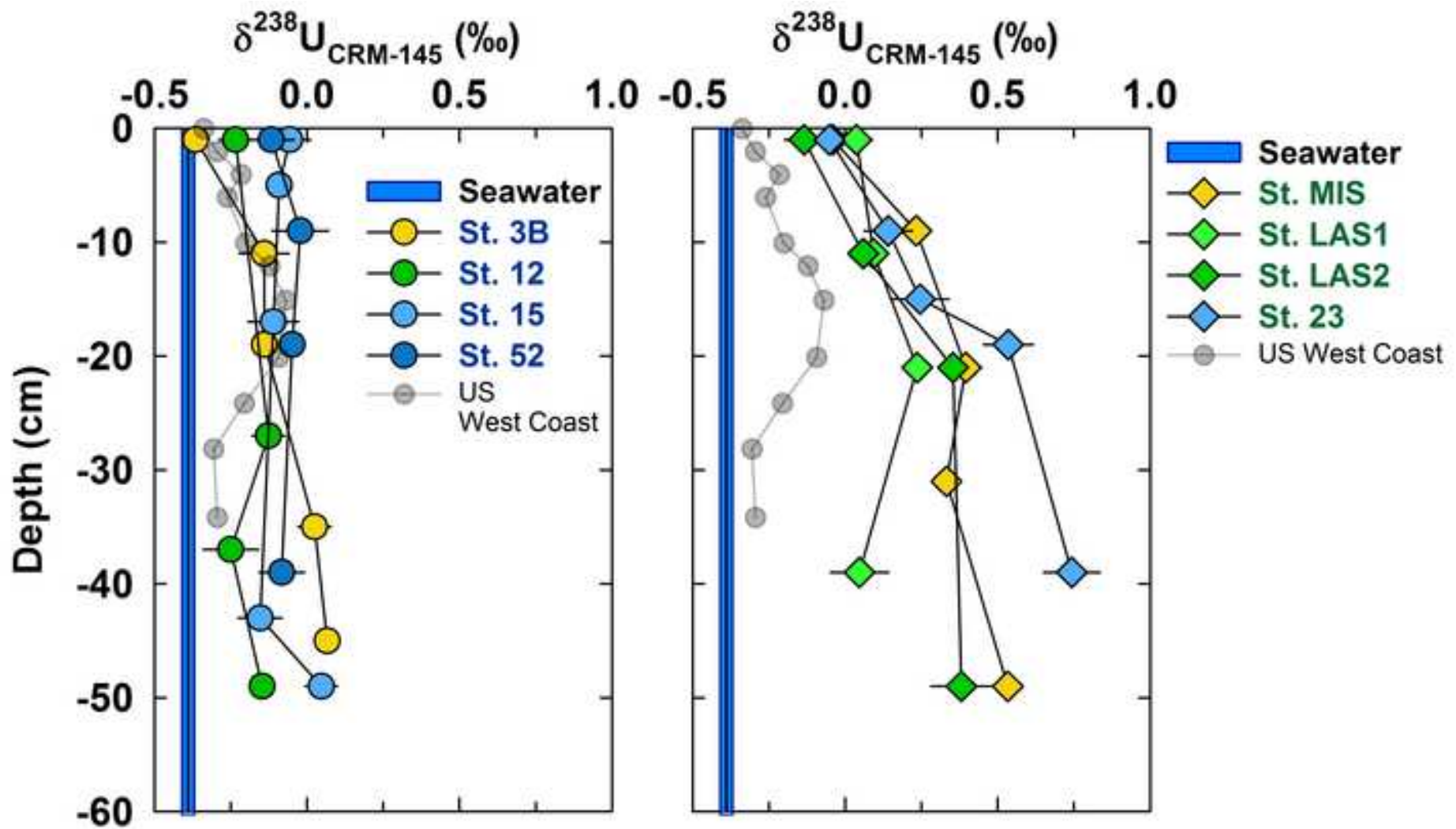


Figure 7  
[Click here to download high resolution image](#)

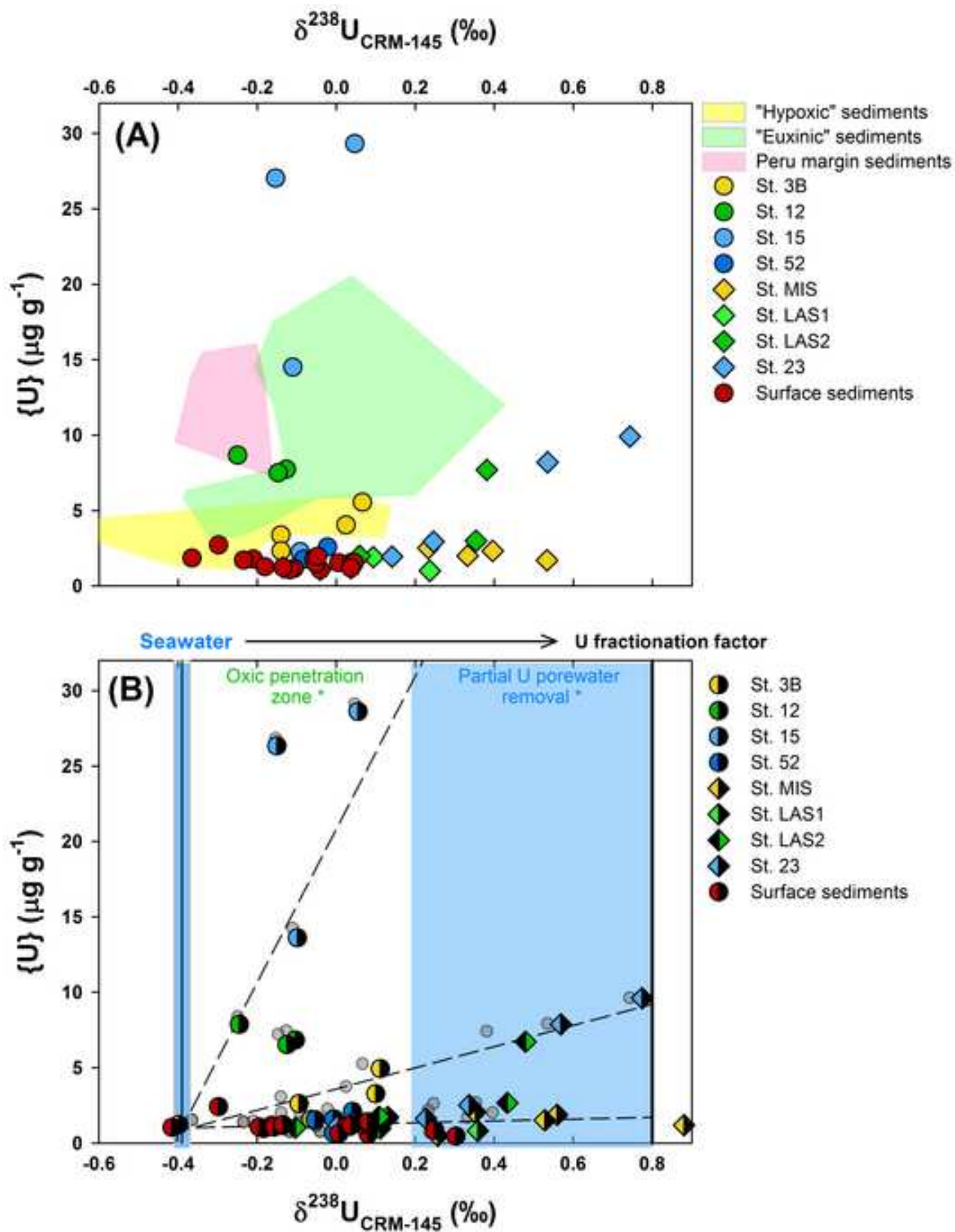


Figure 8

[Click here to download high resolution image](#)

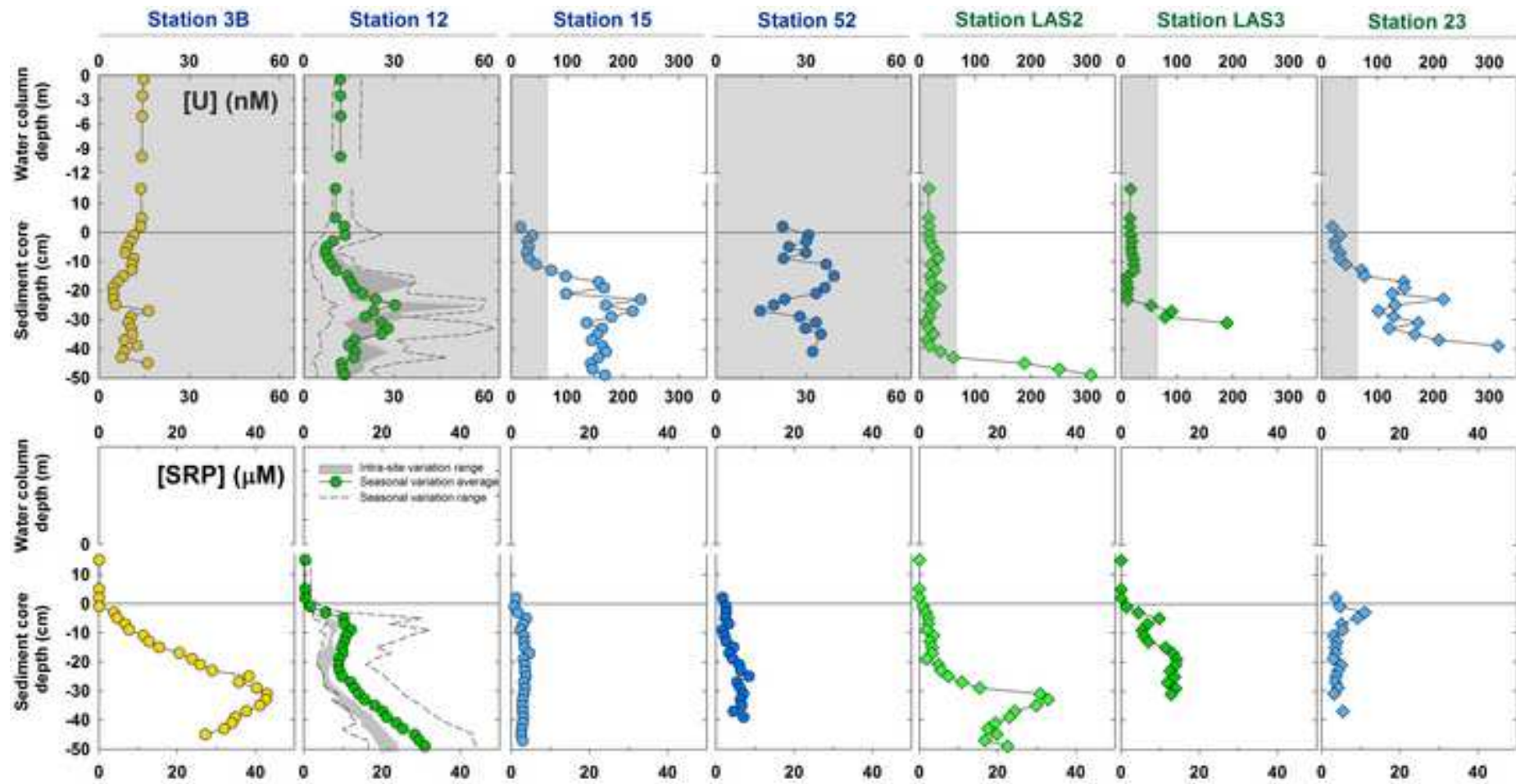


Figure 9

[Click here to download high resolution image](#)

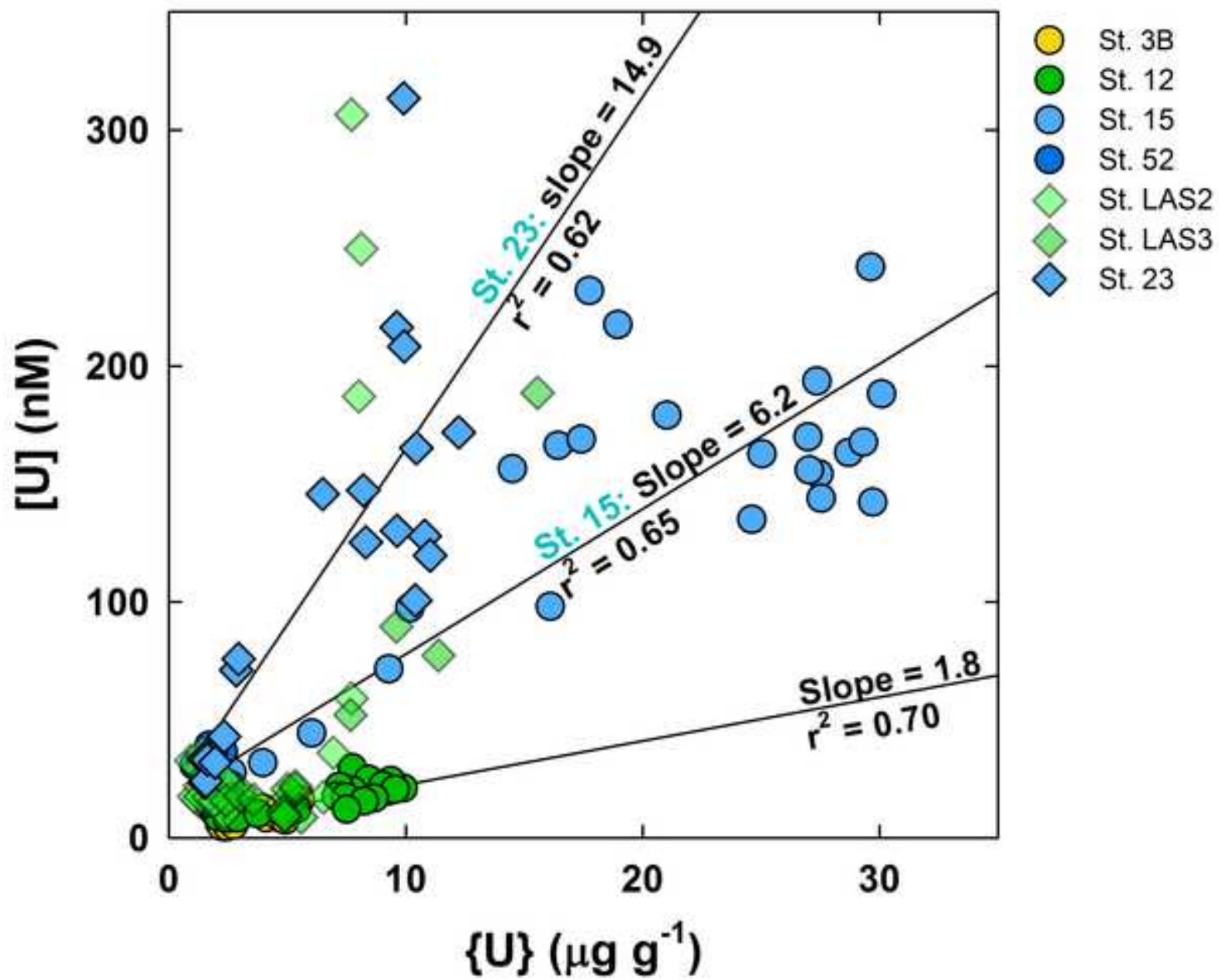


Table 1

[Click here to download Table: Dang et al. Table 1.docx](#)

Table 1:

Stations	23	LAS0	LAS1	LAS2	LAS3	MIS	3B	12	15	52	
Accumulation rate ( $g_U g^{-1} cm^{-1}$ ) (first 10 cm)	0.03	0.10	0.06	0.0	0.4	0.19	0.17	0.24	0.14	0.13	
$r^2$ (linear increase in {U} with depth)	0.99	0.2	0.68	0.2	0.96	0.95	0.86	0.96	0.96	1.00	
Average		0.04 $\pm$ 0.05					0.21 $\pm$ 0.10				
{U <sub>authigenic</sub> } (%) in 0-2 cm sediments	81.3	83.3	82.0	84.0	86.1	46.6	66.0	56.3	62.9	62.2	
Average		83.3 $\pm$ 1.9					58.8 $\pm$ 7.7				
Ti/Al x 100 ( $\pm$ sd)	1.3 (0.3)	3.5 (0.6)	4.9 (0.5)	3.5 (1.1)	2.5 (0.3)	1.5 (0.1)	2.4 (0.2)	0.9 (0.1)	1.1 (0.1)	1.9 (0.2)	

**Supplementary material for online publication only**

**[Click here to download Supplementary material for online publication only: Dang et al. Supplementary information.doc](#)**